It is interesting that even though Eq. 2.17 was derived on classical arguments, it is also correct quantum mechanically. The same result is obtained by an exact solution of the Schrödinger equation for a Coulomb potential†, as well as by a first-order perturbation theory (Born approximation) treatment. We remark also that the same scattering cross section is obtained when the potential is attractive, the two cases being experimentally indistinguishable (as shown in Fig. 6.1). We know, however, that for the electromagnetic force the potential is "attractive" for particles of opposite charge and "repulsive" for particles of the same charge.

2.2 Scattering of Alpha Particles by the Nucleus of Gold

We will now describe in detail a measurement of the scattering of polonium 210 alpha particles from a very thin foil of gold. The apparatus used is, in essence, similar to that of Rutherford's except for the detection technique. As in any scattering experiment we need:

(1) *The beam of particles to be scattered.* The alpha particles (He^4 nuclei) from Po^{210} decay are ideally suited for this purpose, since (a) they have sufficient energy (5.2 MeV) to traverse a thin target; (b) the beam is monoenergetic and does not contain electrons; (c) the high intensity of a radioactive source permits adequate collimation to yield a narrow beam; (d) they are readily available.‡

(2) *The target, or scattering material.* This needs to be sufficiently thick to produce enough scattering events for the available incident-beam intensity; but it should not be so thick as to change appreciably the energy of the primary beam or to affect the scattered alpha particles.§ The target thickness used is of the order of a few mg/cm^2.

(3) *The detector.* In this apparatus a thin piece of scintillating material (organic) mounted onto a photomultiplier was used.¶ Since the range of 5.2-MeV alphas in air is only approximately 4 cm, the beam, scatterer, and detector must all be enclosed in a vacuum. The detector can be moved to different angles with respect to the beam line, so that the angular distribution of the scattered alpha particles may be obtained.

The apparatus is shown in Fig. 6.4a; it consists of the cylindrical vessel A, containing the beam source, target holder, and detector; vessel A can

† See, for example, M. Born, *Atomic Physics*, Hafner Publishing Co., 1957, Appendix XX, p. 360.

‡ To accelerate an alpha particle to this energy one would need a potential difference of 2.6×10^6 eV (Van de Graaf generator) or would have to use a cyclotron.

§ It should not be thicker than a fraction of a mean free path.

¶ A solid-state counter (as described in Chapter 5, Section 5.2) may also be used to detect the alpha particles. It has the advantage of simplicity and better discrimination against background.

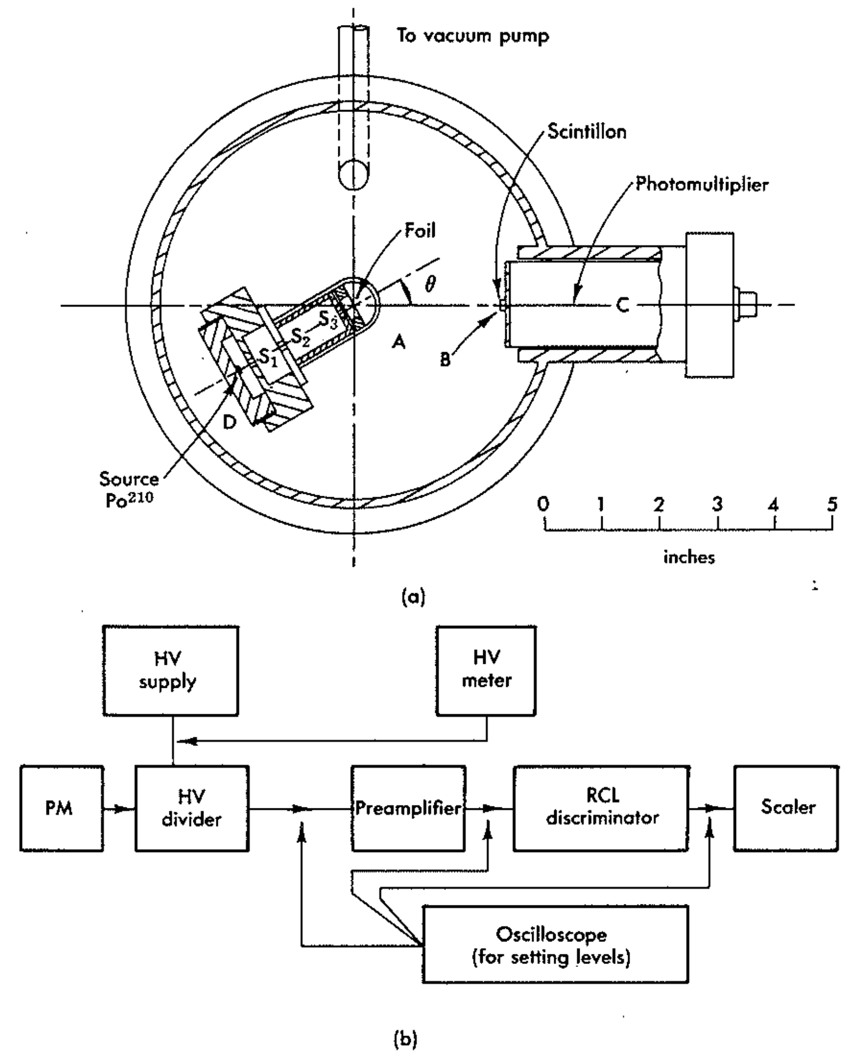

Fig. 6.4 Apparatus used for Rutherford scattering experiment. (a) The scattering chamber, source, target and detector. (b) Block diagram of the electronics.

be readily evacuated. The thin slab of scintillon† B, of width 0.565 cm, height 1.55 cm, and thickness 0.15 cm, is the detecting element, and is glued onto a 6192 DuMont photomultiplier tube C; the photomultiplier is permanently set into the scattering chamber with the vacuum seal made at its plastic base (one should ascertain that the tube does not get drawn

† The material used was Pilot B (Pilot Chemicals, Inc., 36 Pleasant St., Watertown, Mass.).

into the chamber when it is first pumped down). For the beam source, 0.5 millicuries of Po^{210} were plated on the inside of the round cap D, which can be unscrewed easily for removal. Three slits, S_1, S_2, and S_3, 1 mm by 1 cm, are used to collimate the flux of alpha particles emitted by the source. Beyond the third slit, the target holder can be positioned; it consists of a small 2 cm by 2 cm frame on which the scattering foil (gold, aluminum, etc.) is mounted.

Usually the detector is swung around the incident-beam direction. In the present setup, however, it is more convenient to have the detector fixed and to rotate the beam and scattering foil. This latter assembly is mounted as a whole on a shaft coaxial with the scattering center, and can be moved without breaking the vacuum; a pointer outside the chamber indicates the angle of rotation. The associated circuitry (Fig. 6.4b) is the standard one consisting of the high-voltage supply and divider for the photomultiplier, a preamplifier, and an RCL 20506 single-channel discriminator driving a scaler, as described in Chapter 5, Section 4.2.

The counts that register on the scaler do not all come from scattered alpha particles but contain "background" of two types:

(a) A counting rate R'', which is present even when the source is removed from the chamber. This is due mainly to contamination of the chamber with Po^{210}, and to noise in the detector or electronics. To measure R'' the source is removed and a count is taken at different angles; it is usually independent of angle.

(b) A counting rate R' due to the source, but not produced by scattering in the target material itself. The rate R' is mainly due to poor beam collimation, slit scattering, scattering off residual air molecules, and so on. To measure R', the source is placed in position, but the scattering foil is removed and again a count is taken at different angles. This time an angular dependent background may be expected.

Since R' contains R'',† the true rate is given by

$$R_{\text{true}}(\theta) = R(\theta) - R'(\theta) \tag{2.20}$$

where R is the counting rate with both source and target in place. It is necessary to know R' and R'' separately in order to understand the causes of the background and thus reduce it as much as possible.

Let us next make some quantitative estimates on the expected counting rates. The defining beam slit is 1 mm by 1 cm at a distance of 5 cm, and hence subtends a solid angle

$$\Delta\Omega(\text{beam}) = 4 \times 10^{-3}\ \text{sr}$$

† Unless the scattering foil is contaminated, which can be readily ascertained.

We thus obtain for the beam intensity

$$0.5 \times 10^{-3} \times 3.7 \times 10^{10} \times \frac{.004}{4\pi} = 6000\ \text{counts/sec}$$

The observed beam intensity, however, is 110,000 counts/min, the difference from our simple estimate being due in part to the extent of the source but mainly to self-absorption in the source.

Next we consider the detector solid angle. The size of the scintillon is 0.873 cm² at a distance of 6.66 cm, hence

$$\Delta\Omega \sim 0.02\ \text{sr}$$

If we use a gold foil of thickness 0.0001 in., and

$$Z' = 2; \qquad Z = 79; \qquad \text{and} \qquad E = 5.2\ \text{MeV}$$

we obtain†

$$\frac{d\sigma}{d\Omega} = \left[\frac{2 \times 79}{4\pi\epsilon_0} \frac{(1.6 \times 10^{-19})^2}{5.2 \times 10^6 \times 1.6 \times 10^{-19}} \frac{1}{4}\right]^2 \frac{1}{\sin^4 \theta/2} = \frac{1.20 \times 10^{-20}}{\sin^4 \theta/2}\ \text{m}^2$$

Thus for scattering through 15°

$$\frac{d\sigma}{d\Omega}(\theta = 15^\circ) = 4.17 \times 10^{-21}\ \text{cm}^2$$

The number of alphas scattered into the detector is given by

$$I_s = I_0 N \frac{d\sigma}{d\Omega} d\Omega$$

where

$I_0 = 1.1 \times 10^5$ counts/min in the incident beam

$d\Omega = 2 \times 10^{-2}$ sr

$N = t \times \rho \times (N_0/A)$, the area density of scatterers, where

$N_0 = 6 \times 10^{23}$, Avogadro's number

$\rho = 19.3$ gr/cm³, the density of the scatterer (gold)

$t = 0.00025$ cm, the thickness of the foil

$A = 197$, the atomic weight of gold

† Note that we calculate in the MKS system and that dimensionally

$$[(Z^2e^2)/(4\pi\epsilon_0)]^2 = [F]^2[L]^4 \qquad \text{while} \qquad E^2 = [F]^2[L]^2$$

This yields

$$N = 1.48 \times 10^{19} \text{ gold nuclei/cm}^2$$

and

$$I_s(\theta = 15°) = 132 \text{ counts/min}†$$

This seems to be a sizable rate; however, the pertinent question is how this rate compares to the background rate R'; that is, what is the signal-to-noise ratio (S/N). In the present experiment, the background (mainly due to the contamination of the vessel) was high, and of the order of 130 counts/min; thus already at 15°, $S/N = 1$.

To improve the S/N ratio, we could increase I_s by increasing the solid angle (which is impractical), or by increasing the beam intensity (which might raise the noise level as well) or most simply, by increasing the scattering-foil thickness. If we increase the foil thickness, however, we are limited by the energy loss of the beam particles in the target. If we wish, for example, to determine the cross section to 25 percent, then since

$$\frac{d\sigma}{d\Omega} \propto E^{-2}$$

and

$$\frac{\Delta(d\sigma/d\Omega)}{d\sigma/d\Omega} = -2\frac{\Delta E}{E}$$

the energy loss must not exceed 12 percent. By referring to the Bragg curve (Fig. 5.42) we note that a 5.2-MeV alpha particle will lose 1.5 MeV of its energy after traversing the equivalent of 1.2 cm of air at stp, namely, approximately 2 mg/cm², which corresponds to a gold foil of thickness $t = 0.00012$ cm.‡

Multiple scattering in the foil is not significant for the alpha particles. We use Eq. 2.17, Chapter 5, and $L_{rad} \approx 6$ gr/cm² for gold; then with the above value $t = 0.00025$ cm, we obtain

$$\theta_{rms} = \frac{21.2}{\sqrt{2mE}} Z^2 \sqrt{\frac{10^{-3}}{6}} \text{ rad} \simeq 0.25°$$

† $I_s(\theta = 15°) = 1.1 \times 10^5 \times 1.5 \times 10^{19} \times 2 \times 10^{-2} \times 4 \times 10^{-21}$.

‡ From Chapter 5 we see that energy loss/(gm/cm²), $dE/d\xi = N_0(Z/A)z^2f(I, \beta)$, yielding the equivalent thickness of gold $t = 0.00012$ cm. However, at these low velocities a more detailed treatment of the energy loss is required, and as also observed experimentally the alpha particle loses 1.5 MeV after traversing a gold foil of thickness $t = 0.00025$ cm (see also Fig. 5.4).

2.3 Results and Discussion

We now will give results for Rutherford scattering obtained by students† with the apparatus described in Section 2.2.

It is important to be extremely careful when handling the radioactive source for this experiment; polonium, while very convenient for Rutherford scattering, is a "nasty" isotope. As noted in Chapter 4, it can be lethal when taken internally, and due to the recoil following alpha emission, small parts of the source break off and contaminate the vessel in which it is enclosed. Further, alpha-particle contamination cannot be detected with a Geiger counter, but only with special alpha detectors, such as a gas-flow counter‡. *Gloves must always be worn* when handling the source, and the cap must be replaced whenever the source is removed from the apparatus.

First the chamber is evacuated and the detection system is adjusted with the source in place, but without the scattering foil. The detector is placed at 0° and the photomultiplier output is observed on an oscilloscope; the high voltage is then raised until clean pulses of a few volts amplitude are obtained. Next the discriminator is adjusted by taking a plateau curve in the integral mode; it is also possible to operate the discriminator in the differential mode, but in either case attention must be paid to the energy loss of the alphas when the foil is inserted.

We are now in a position to measure the beam profile when the scatterer is *not* in place; the results of counting rate against angle are shown on a linear scale in Fig. 6.5a and on a logarithmic scale in Fig. 6.5b. This measurement serves three purposes:

(a) It determines the background rate R' and gives the extent of the beam, namely, the detector angles beyond which the counts will be due to scattered alphas. From Fig. 6.5b we see that for $\theta \gtrsim 6°$ there are no beam counts; also the value of the background is 130 counts/min. (As noted earlier, this rate was due almost entirely to contamination of the chamber, as evidenced by a separate measurement with the source removed).

(b) It provides the information on the incoming beam intensity, and for this purpose the linear plot of Fig. 6.5a is more useful. If the over-all beam dimensions are smaller than the dimensions of the detector, then the peak count simply gives the beam intensity and the profile of Fig. 6.5a should have a flat top.

This is not always true, however. Let us first consider the distribution of the beam in the θ direction (horizontal); this may be uniform, or Gaussian, or of another type. Let the interval $\Delta\theta = x$ contain 90 percent of the beam

† R. Dockerty and S. McColl, class of 1962.

‡ PAC 3G Gas Proportional Counter; may be purchased from Eberlein Instruments Corp., Sante Fé, N. M.

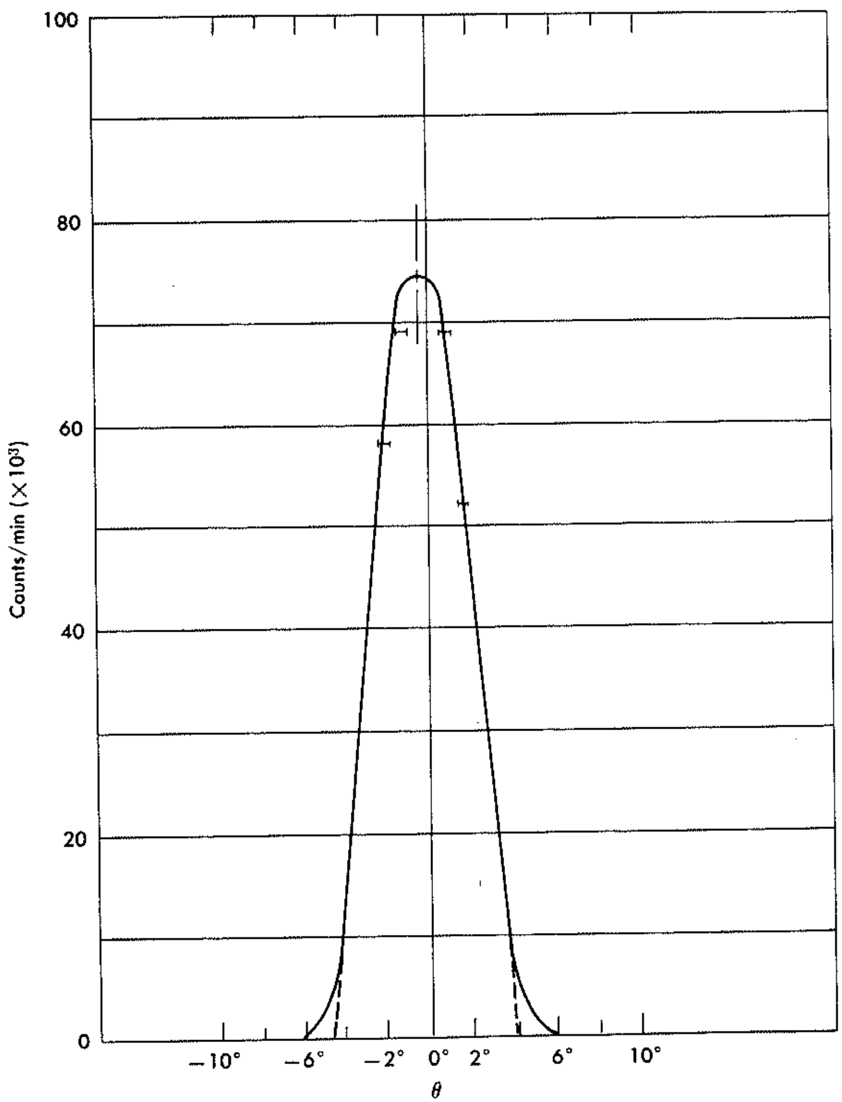

(a)

FIG. 6.5 The profile of the alpha-particle beam as measured in the scattering chamber with the scattering foil removed. (a) (*Above*) Linear plot that is used for obtaining the total flux, and the beam center. (b) (*Opposite page*) Semilogarithmic plot giving the background level outside the beam.

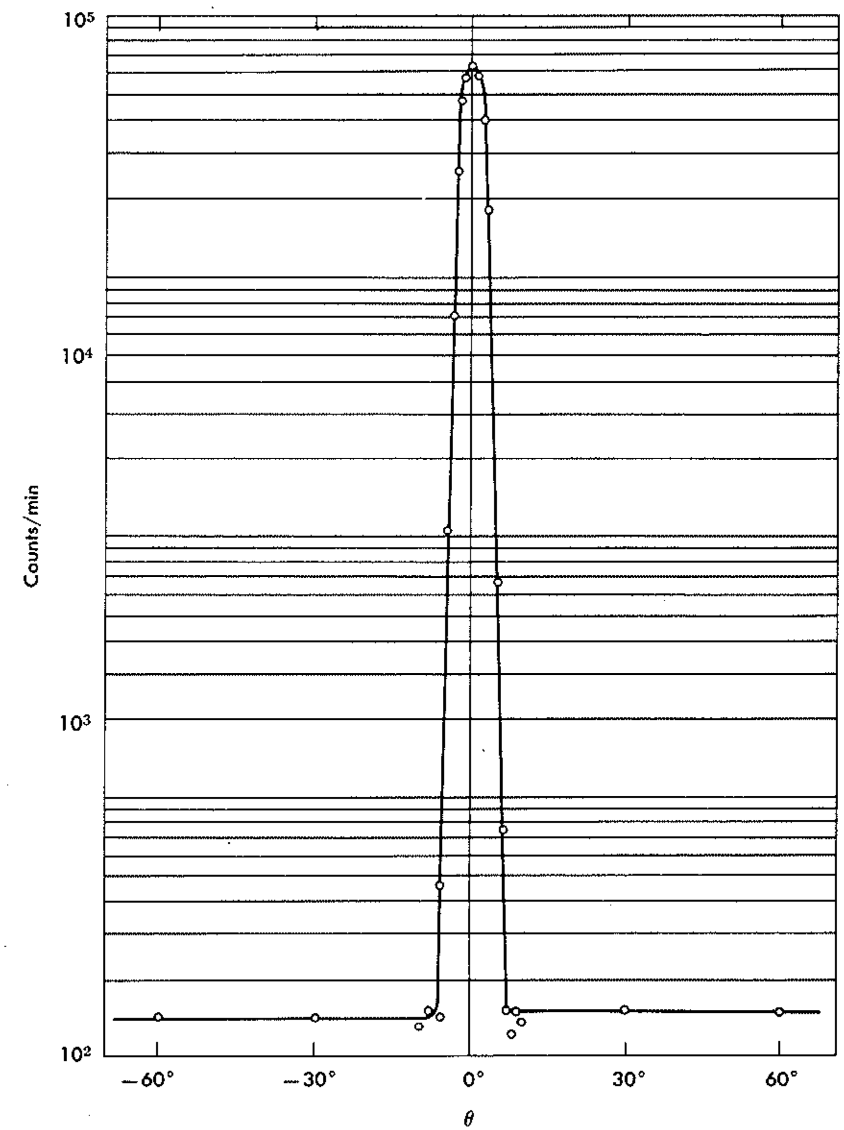

(b)

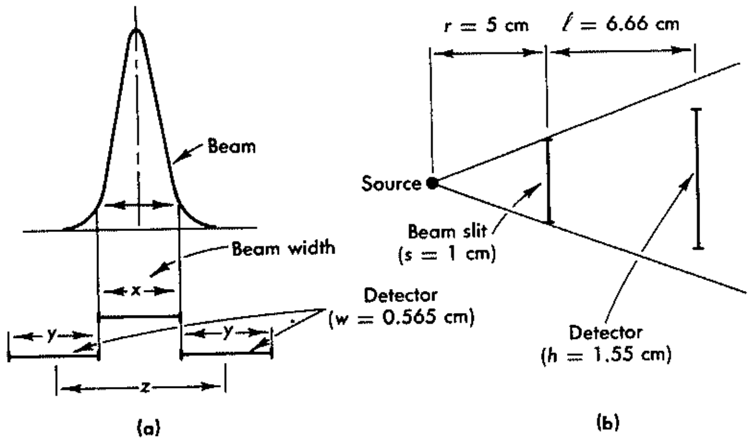

FIG. 6.6 The effects of the finite dimensions of the beam and of the detector. (a) In the horizontal plane. (b) In the vertical plane.

(see Fig. 6.6a). The angular width of the detector is

$$\Delta\theta = y = \frac{0.565}{6.66} \times \frac{180}{\pi} = 4^\circ\!.9$$

Further, from Fig. 6.5a we observe that the beam counts drop to 10 percent of their peak value in $\Delta\theta = z = 8^\circ\!.5$ (by extrapolating to zero beam count, we obtain $\Delta\theta = z' = 9^\circ$). As seen in Fig. 6.6a, $z = x + y/2 + y/2$, so that we find $x \simeq 3^\circ\!.6$, which is smaller than the detector width; consequently we must expect in the profile of Fig. 6.5a a flat top of width $\Delta\theta = y - x \approx 1^\circ\!.3$.

Unfortunately in the vertical direction, the beam size is larger than the dimension of the detector, as is seen in Fig. 6.6b, where the dimensions of the beam-defining slit and the detector are shown. We note that only a fraction F of the incident beam reaches the detector, where

$$F = \left(\frac{h}{s}\right)\left(\frac{r}{r + l}\right) = 0.665$$

Thus the total incident beam is given by

$$I_0 = \frac{I_\theta}{F} = 110{,}000 \text{ counts/min}$$

where I_θ is the peak counting rate obtained from the beam profile, which we took as $I_\theta = 74{,}000$ counts/min. The above value of I_0 is subject to at least a ± 20 percent error in view of the approximations used and the nonuniformities in beam density and direction.

(c) Finally, the beam profile gives information on the true position of the beam axis. From Fig. 6.5a we find that the axis is located at $\theta_0 = -0^\circ\!.25$, and all the scattering angles must be corrected accordingly.

Now data may be taken. The chamber is opened, the scattering foil inserted, and the chamber again evacuated. The counting rate is measured as a function of angle first to the one side and then to the other side of the beam. These raw data are given in column 2 of Table 6.2. Column 3 gives the counts after background subtraction and column 4 the probable error; in column 5 are shown the corrected angles. At each angle enough data are accumulated so that the statistical accuracy is of the order of 3 percent.

In evaluating columns 3 and 4, the background rate R' was taken as 130 ± 10 counts/min (see Fig. 6.5b). The large error on the background is not due to a statistical uncertainty (which could be reduced) but to fluctuations in R' over the period that the experiment was in progress. As R becomes comparable to R', the error in the true rate $R_t = R - R'$ increases, reaching $\Delta R_t/R_t \approx 0.5$, which sets a limit to the largest useful scattering angle.

From the observed yields of scattered particles, we can obtain the differential cross section, from the expression

$$\frac{d\sigma}{d\Omega} = \frac{I_s}{(\Delta\Omega) I_0 N}$$

where the symbols are defined as on page 239 and have the same values

$I_0 = 110{,}000$ counts/min
$N = 1.48 \times 10^{19}$ gold nuclei/cm² (for the given thickness of the foil $t = 0.00025$ cm)
$\Delta\Omega = 0.02$ sr (but see next paragraph)
$I_s =$ value given by column 3 of Table 6.2

The differential cross section so obtained is shown in column 6 of Table 6.2 and is also plotted against the scattering angle in Fig. 6.7a.

The process of dividing the yield by $\Delta\Omega$ to obtain the cross section needs some further discussion. Two points are of special importance:

(a) In evaluating $\Delta\Omega$ we use the approximation

$$\Delta\Omega = \frac{hw}{l^2} = \frac{1.555 \times 0.565}{(6.66)^2} = 0.0197 \text{ sr} \tag{2.21}$$

where w and h are the width and height of the rectangular detector and l the distance from the target (see also Fig. 6.6). The approximation is valid because the detector area is always normal to the scattered beam, and

TABLE 6.2
RUTHERFORD SCATTERING DATA

θ_{dial} (1)	R (counts/min) (2)	$R - R'$ (3)	$\Delta(R - R')$ (4)	θ_{correct} (5)	$d\sigma/d\Omega$ (observed) (6)	$(\sin^4 \theta/2)^{-1}$ (7)	k (8)
					$\times 10^{-21}$ cm²/sr	$\times 10^3$	$\times 10^{-24}$ cm²/sr
−70°	144.3						
−60°	147.2						
−50°	139.8						
−40°	148.6						
−35°	145.2						
−30°	144.2						
−25°	166.6	37	±15	24°45′	1.13	0.460	2.46
−20°	228.6	99	±15	19°45′	3.04	1.16	2.62
−15°	443	313	±17	14°45′	9.60	3.72	2.59
−10°	1868	1738	±40	9°45′	53.4	19.2	2.78
−8°	5336	5206	±72	7°45′	160	47.9	3.34
0°	41662						
+6°	8576	8146	±90	6°15′	250	115	2.17
+8°	3663	3533	±60	8°15′	107	37.5	2.85
+10°	1681	1551	±40	10°15′	47.6	15.7	3.04
+15°	380	250	±17	15°15′	7.68	3.24	2.37
+20°	215.7	86	±15	20°15′	2.54	1.05	2.42
+25°	182.2	52	±15	25°15′	1.60	0.437	3.66
+30°	161.6	32	±15	30°15′	0.98	0.190	
+35°	163.2						
+40°	132.7						
+50°	142.1						

it becomes better as l increases, and the beam spot on the target decreases. More accurately, we must integrate the element of solid angle

$$d\Omega = \sin\theta \, d\theta \, d\varphi$$

over the area of the detector. Clearly, if we approximate and assume θ to be constant, $d\theta = \Delta\theta = w/l$, and $d\varphi = \Delta\varphi = h/(l \sin\theta)$, we obtain Eq. 2.21, which is independent of θ.

(b) In dividing the yield by $\Delta\Omega$ to obtain the differential cross section we must assume that $d\sigma/d\Omega$ does not change appreciably over the angular range subtended by the detector. This assumption is not very good, especially at the smaller scattering angles. Correctly, we should integrate $d\sigma/d\Omega$ over $d\Omega$ to obtain the yield

$$I = \int_{\varphi_1}^{\varphi_2} d\phi \int_{\theta_1}^{\theta_2} \frac{1}{\sin^4 \theta/2} \sin\theta \, d\theta = \frac{4}{2}(\varphi_1 - \varphi_2) \left. \frac{1}{\sin^2 \theta/2} \right]_{\theta_1}^{\theta_2}$$

but we may set $\varphi_1 - \varphi_2 \simeq h/(l \sin\bar{\theta})$ as before, and

$$I = \frac{h}{l \sin\bar{\theta}} \left[\frac{\sin^2(\theta_1/2) - \sin^2(\theta_2/2)}{\sin^2(\theta_1/2)\sin^2(\theta_2/2)} \right]$$

which approximates but is not equal to the result obtained by using Eq. 2.21

$$I = \frac{hw}{l^2} \frac{1}{\sin^4 \bar{\theta}/2}$$

In order to compare the results with the theoretical prediction of the Rutherford cross section (Eq. 2.17) we give in column 7 of Table 6.2 the factor $(1/\sin^4 \theta/2)$ evaluated at the appropriate angle. The observed cross section should be proportional to this factor, and column 8 gives the ratio $k =$ (column 6)/(column 7), which should be equal to

$$k = \left(\frac{zZe^2}{4\pi\epsilon_0} \frac{1}{4E} \right)^2 \tag{2.22}$$

In Fig. 6.7b is a log-log plot† of yield against $1/(\sin^4 \theta/2)$; horizontal error bars correspond to $\pm 0^\circ\!.25$ uncertainty in the scattering angle,‡ while the vertical ones correspond to the errors given in column 4 of Table 6.2. Angles to the right of the beam axis are indicated by a cross, to the left of the axis by a circle.

† On a linear scale, the plot should yield a straight line of slope k. However, on the log-log plot we cover a much larger range of values; the slope of the line must be 1 and the intercept gives k.

‡ Remember, however, that the detector angular width is $\pm 2^\circ\!.5$.

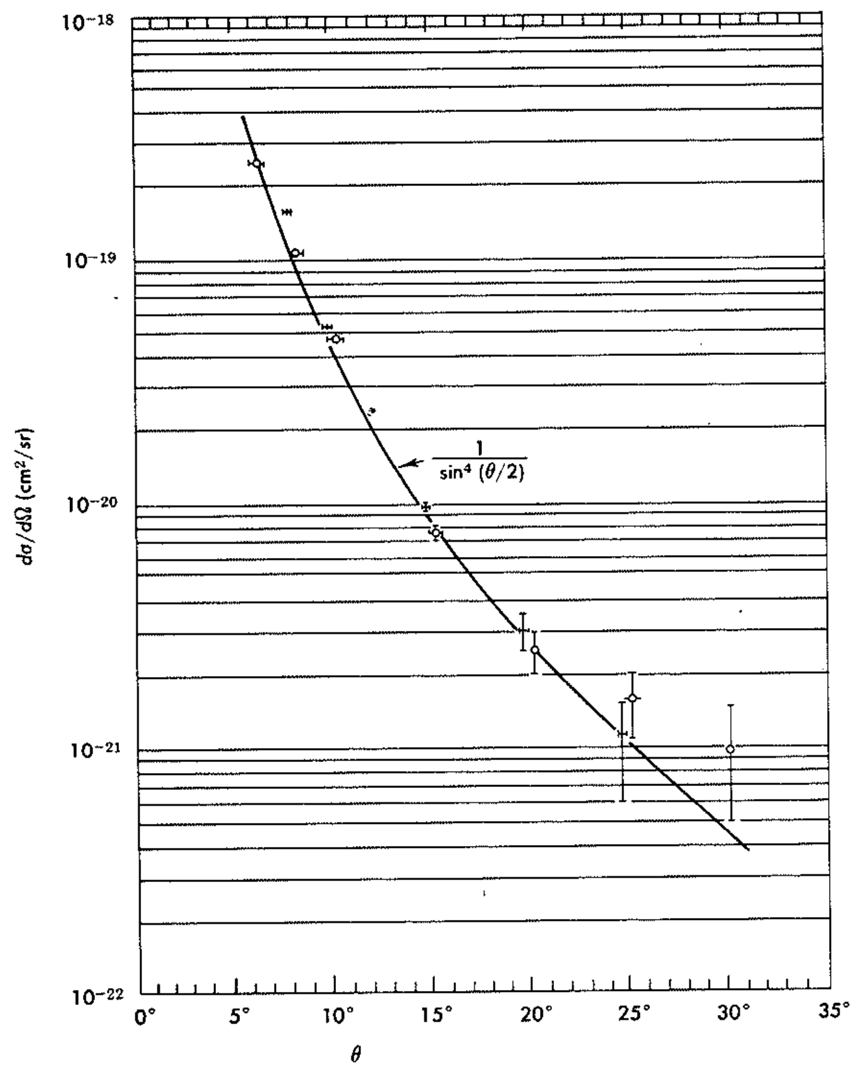

(a)

FIG. 6.7 Results of the Rutherford scattering experiment. (a) Cross section against angle; note that the measurement is extended over three decades. (b) Cross section against $1/(\sin^4 \theta/2)$; note the straight line fit and the unit slope of the line.

The straight line on Fig. 6.7b is the theoretical prediction that has slope = 1.00. We note that it provides a very good fit to the experimental points over more than two decades, and therefore these data confirm the

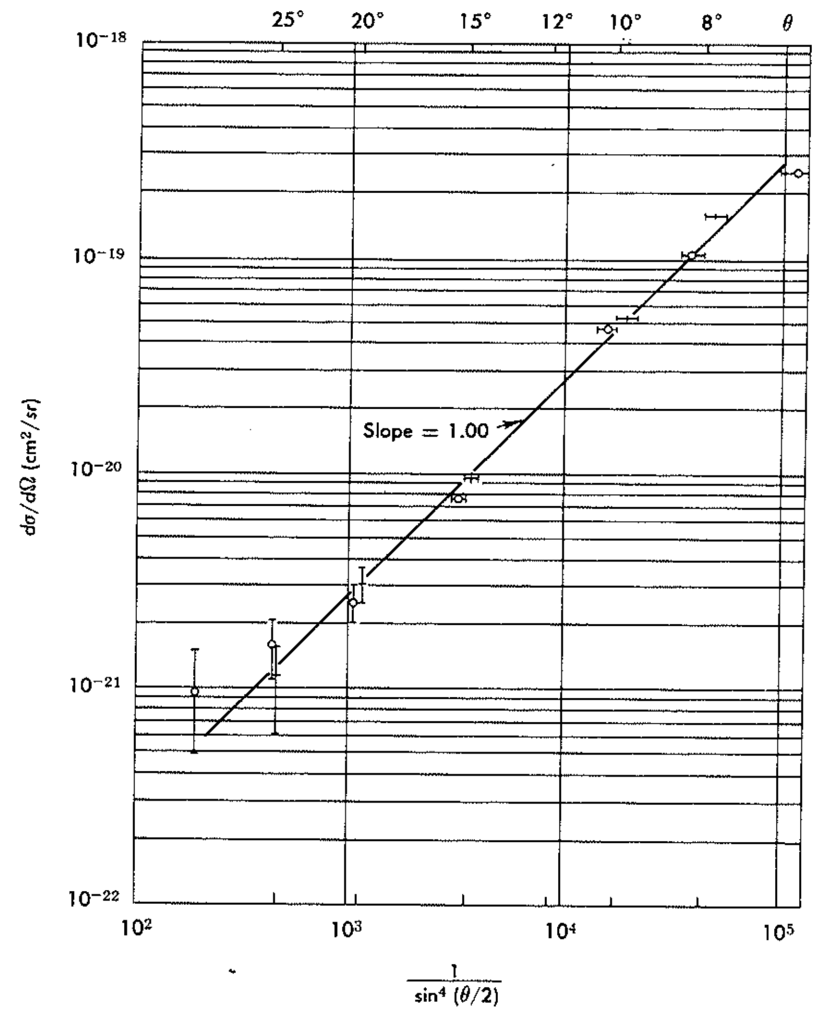

(b)

hypothesis of the nuclear atom and the angular dependence of the Rutherford scattering cross section as obtained in Eq. 2.17. The small deviations from the fit are due to experimental difficulties which will be discussed below.

While the straight line in Fig. 6.7b was constrained to have slope = 1.00, the intercept (that is, the normalization) was obtained by a least-squares fit to the data points. It yields a value

$$k = 2.70 \times 10^{-24}\ \text{cm}^2$$

Evaluation of Eq. 2.22 with $E = 5.2$ MeV yields $k = 1.20 \times 10^{-24}$ cm^2. However, the alpha particle loses a considerable amount of energy when traversing the target; it is therefore more appropriate to average $1/E^2$ over this energy range, that is,

$$\left\langle \frac{1}{E^2} \right\rangle = \frac{\int_{x_1}^{x_2} E^{-2}\, dx}{\int_{x_1}^{x_2} dx}$$

We assume for simplicity that the energy loss is proportional to the thickness

$$E = E_0 - \left(\frac{dE}{dx}\right)x$$

hence

$$dE = -\left(\frac{dE}{dx}\right) dx$$

and we can write

$$\left\langle \frac{1}{E^2} \right\rangle = \frac{\int_{E_1}^{E_2} E^{-2}\, dE}{\int_{E_1}^{E_2} dE} = \frac{1/E_1 - 1/E_2}{E_2 - E_1} = \frac{1}{E_1 E_2}$$

We now use $E_1 = 5.2$ MeV, $E_2 = 3.7$ MeV, and obtain from Eq. 2.22

$$k = 1.67 \times 10^{-24} \text{ cm}^2 \text{ (theory)}$$

whereas

$$k = 2.70 \times 10^{-24} \text{ cm}^2 \text{ (experiment)}$$

The difference between the observed and theoretical constants, while at first sight large, can be traced to the limited sensitivity of the apparatus and mainly to

(a) Uncertainty in incoming flux
(b) Uncertainty in foil thickness

and to a lesser extent to

(c) Extended size of the beam and lack of parallelism
(d) Extended angular size of the detector
(e) Plural scattering in the foil (for the data at small angles)
(f) Background (for the data at large angles)

The reader should keep in mind that the main purpose of the experiment was to prove the $1/(\sin^4 \theta/2)$ dependence. Further, the observed value of k is of the correct order of magnitude and if we used it to find the charge of the gold nucleus, we would obtain

$$Z' = 99 \qquad \text{instead of} \qquad Z = 79$$

It is interesting to note that when the foil was inserted, the counting rate at 0° dropped from $I_0 = 74{,}000$ to $I_0' = 41{,}660$ counts/min (see Table 6.2). This reduction is a measure of the total cross section, or more precisely of

$$I_0 - I_0' = \sigma_t N I_0 = N I_0 \int_{\theta_0}^{\pi} \frac{d\sigma}{d\Omega}(\theta)\, d\Omega$$

where for θ_0 we use the angular limits of the detector.† Then we obtain for the probability of interaction (see Eq. 2.19)

$$\frac{I_0 - I_0'}{I_0} = Nk \frac{2\pi}{\sin^2 \theta_0/2}$$

With $\theta_0 = 2.°5$, $N = 1.48 \times 10^{19}$, and the observed value of

$$\frac{I_0 - I_0'}{I_0} = 0.44$$

we obtain

$$k = 2.26 \times 10^{-24} \text{ cm}^2$$

which is of the correct order of magnitude. However, in view of the crude approximations made in evaluating the total cross section, the agreement with the previously discussed values of k is fortuitous.

The large value for $(I_0 - I_0')/I_0$ indicates that the probability for scatters $\geq 2.°5$ is considerable, and that therefore it is probable that an alpha particle may suffer in traversing the foil more than one (small angle) scattering from a nucleus.

We conclude this section with two further remarks:

(a) If we changed the scattering material, the cross section would also change, as $(Z/Z')^2$, while maintaining the same angular dependence. We can thus obtain information on the charge of the nucleus and confirm that it is equal to the atomic number Z of the material. Convenient target materials are silver, $Z = 47$, aluminum, $Z = 13$, and others.

† This discussion is really applicable to a beam of circular cross section and to a circular detector.